Indian Journal of Geo Marine Sciences
Vol. 49 (04), April 2020, pp. 634-640

An improved technique for SAR internal wave signal detection

K Fan[a,b], Y Gu[*,b], H Zhang[c], C Li[a] & X Yu[d]

[a]32021 Army, PLA, Beijing – 100 094, China

[b]College of Physical and Environmental Oceanography, Ocean University of China, Qingdao – 266 100, China

[c]State Key Laboratory of Satellite Ocean Environment Dynamics, Second Institute of Oceanography, State Oceanic Administration, Hangzhou – 310 012, China

[d]Faculty of Resources and Environmental Science, Hubei University, Wuhan – 430 062, China

*[Email: guyanzhen@ouc.edu.cn]

Received 19 September 2018; revised 09 November 2018

One improved boundary process method for synthetic aperture radar (SAR) internal wave signal detection, which tries to reduce the errors during the extending process for empirical mode decomposition (EMD), has been introduced in this paper. This method is based on EMD and the criterion created by the theory that the max normalized deflection stands for the largest energy. The method was first applied both on several time series decompositions and on SAR nonlinear internal wave temporal series decompositions. The comparison of results showed that this method was more feasible and precise indicating that the method can detect the internal wave signals successfully from SAR image even with a lot noise.

[Keywords: Empirical mode decomposition, Hilbert-Huang transform, Internal wave, Synthetic aperture radar]

Introduction

Internal waves are major dynamic features, which travel within the interior of the ocean[1,2]. Internal wave fields are measured by instruments deployed in the ocean, like temperature and salinity sensors or current meters, or by acoustic instruments like sonar. However, information on internal wave fields could also be extracted from their sea surface manifestations[3].

Recently, synthetic aperture radar (SAR) has demonstrated the potential to obtain high-resolution ocean surface images from which internal wave features could be identified[4-6]. Such as the distribution and the wavelength of internal wave could be directly extracted from SAR images[7,8], and also the internal wave parameters, such as pycnocline depth and the amplitude could also be retrieved from SAR image[3,9]. Therefore, it is adequate for quantitative estimates of internal wave parameters from SAR images, and the ability to retrieve accurate internal wave parameters from SAR image is especially significant in SAR technique for ocean internal wave research.

However, SAR technique for ocean internal wave parameters retrieval is based on the internal wave signals detection quantitative, but it is hard for us to detect internal wave signals for SAR images with a lot noise. In this paper, one improved boundary process method for nonlinear data analysis is being introduced. This method is based both on empirical mode decomposition (EMD), which was firstly proposed by Huang *et al*. in 1998(ref. 10) and improved in 1999(ref. 11), and on the criterion created by the theory that the max normalized deflection stands for the largest energy.

EMD can break down both the signals to a series of zero-mean intrinsic mode functions (IMFs) that satisfy two conditions: (1) in the whole data set, the number of extrema and the number of zero crossings must either be equal or differ at most by one; and (2) at any point, the mean value of the envelope defined by the local maxima and the envelope defined by the local minima approach is zero. These two characteristics are also the criteria for sifting processes and for EMD to stop. Each sifting process has two steps: (1) construct upper and lower envelopes by connecting all maxima and all minima with cubic splines; (2) subtract the mean of the upper and lower envelopes from the original signal to get a component. The sifting process should usually be applied several times because the component created by only one sifting process hardly satisfies all the requirements of an IMF. Once an IMF is created, the same procedure is then applied on the residual of the signal to obtain the next IMF; the later IMF has the

lower frequency. The decomposition will stop when no more IMFs could be created or the residual is less than a predetermined small value. The results for the decomposition of data could be written as:

$$X(t) = \sum_{i=1}^{M} IMF_i + r(t) \quad \ldots (1)$$

The IMFs yield instantaneous frequencies as a function of time with the Hilbert transform. The whole procedure, EMD and Hilbert transform, composes a new signal process technology called the "Hilbert-Huang transform" (HHT). The HHT proves to be remarkably effective. Many people have applied this method to the analysis of time series data and EMD development[12-27].

After the time series and temporal series decomposed by EMD, the signal is divided into n IMFs. Then we have to pick up one signal from these IMFs. According to the Wave Energy theory: the more the deflection, the more energy the signal contains[28]. As we know, the internal wave signal contains the largest energy. Therefore, the IMF that contains the largest deflection is just the internal wave signal. We calculate the normalized deflection of each IMF based on the following equation:

$$\sigma_i = s_i / \sum_{i=1}^{m} s_i \quad \ldots (2)$$

Where s_i is the standard deviation of the i^{th} component IMF_i. Based on the IMF component picked up, which has the largest deflection, the peaks and troughs locations of the IMF component could be estimated, and then the wavelengths of the internal waves and other internal wave parameters could be retrieved.

However, during the sifting process, the ends of the series cannot be both maximum and minimum. There is a serious problem of spline fitting at the end, where cubic splines can have wide wings if left free. Some extending methods have been proposed recently. Two representational methods are called the mirror periodic extending method (MPM) and the extrema extending method (EEM)[29]. If the time series has a strong asymmetric waveform, the MPM cannot work and it is hard to decide the characteristic period too. Therefore, it is complicated to apply the EEM for a complex series with a lot of noise[22]. Moreover, the worse thing is that wrongly extending the characteristic period leads to a wrong data source for the next sifting process.

In this paper, we present one improved boundary process method, which tries to reduce the errors during the extending process for empirical mode decomposition (EMD). This method is based on EMD proposed by Huang *et al.*[10] and the criterion created by the theory that the max normalized deflection stands for the largest energy, and the method is applied to time series decompositions and SAR nonlinear internal wave temporal series decompositions.

Materials and Methods

One improved fixing the end method (FEM) that fix the end characteristic wave rather than extend the characteristic period during the spline fitting process is introduced in this paper. Its main process is as follows:

$$t = [t_1, t_2, \cdots, t_n] \quad \ldots (3)$$

$$X(t) = [x_1, x_2, \cdots, x_n] \quad \ldots (4)$$

Presume time series $X(t)$ contains p maxima and q minima, their values and indices are designated as ($\mathbf{PV}, \mathbf{QV}$) and ($\mathbf{PI}, \mathbf{QI}$):

$$\mathbf{PI} = [\mathbf{PI}_1, \mathbf{PI}_2, \cdots, \mathbf{PI}_p] \quad \ldots (5)$$

$$\mathbf{QI} = [\mathbf{QI}_1, \mathbf{QI}_2, \cdots, \mathbf{QI}_q] \quad \ldots (6)$$

$$\mathbf{PV} = [X(\mathbf{PI}_1), X(\mathbf{PI}_2), \cdots, X(\mathbf{PI}_p)] = [\mathbf{PV}_1, \mathbf{PV}_2, \cdots, \mathbf{PV}_p] \quad \ldots (7)$$

$$\mathbf{QV} = [X(\mathbf{QI}_1), X(\mathbf{QI}_2), \cdots, X(\mathbf{QI}_q)] = [\mathbf{QV}_1, \mathbf{QV}_2, \cdots, \mathbf{QV}_q] \quad \ldots (8)$$

Let the values and indices of extending maxima and minima be written as:

$$\mathbf{PI} = [t_1', \mathbf{PI}_1, \mathbf{PI}_2, \cdots, \mathbf{PI}_p, t_n'] \quad \ldots (9)$$

$$\mathbf{QI} = [t_1', \mathbf{QI}_1, \mathbf{QI}_2, \cdots, \mathbf{QI}_q, t_n'] \quad \ldots (10)$$

$$\mathbf{PV} = [\mathbf{PV}_0, \mathbf{PV}_1, \mathbf{PV}_2, \cdots, \mathbf{PV}_p, \mathbf{PV}_{p+1}] \quad \ldots (11)$$

$$\mathbf{QV} = [\mathbf{QV}_0, \mathbf{QV}_1, \mathbf{QV}_2, \cdots, \mathbf{QV}_q, \mathbf{QV}_{q+1}] \quad \ldots (12)$$

The end point values are:

$$\mathbf{PV}_0 = \max(x_1, \mathbf{PV}_1) \quad \ldots (13)$$

$$\mathbf{PV}_{p+1} = \max(x_n, \mathbf{PV}_p) \quad \ldots (14)$$

$$\mathbf{QV}_0 = \min(x_1, \mathbf{QV}_1) \quad \ldots (15)$$

$$\mathbf{QV}_{q+1} = \min(x_n, \mathbf{QV}_q) \quad \ldots (16)$$

The generation determination of t_1' can be showed in Figure 1(a). Let L1 = abs ($\mathbf{PI}_1$ - $\mathbf{QI}_1$), L2 = min (abs ($\mathbf{PI}_1$ - t_1), abs ($\mathbf{QI}_1$ - t_1)). Then we get $t_1' = t_1 - (\text{L1-L2})$. However, some exception situations as show in Figures 1(b - c) should be treated exception when the end point value at t is considered as maxima or minima (Fig. 1b) and L2 is larger than L1 (Fig. 1c). In the case of Figure 1(b), we have $t_1' = t_1$. In the case of Figure 1(c), a mirror like extending method is used (not a real mirror), let $t_1' = t_1 - \text{L2}$, then equations (13) and (15) is $\mathbf{PV}_0 = \max(x_1 - \mathbf{QV}_1)$ and $\mathbf{QV}_0 = \min(x_1 - \mathbf{PV}_1)$, respectively. After the first characteristic wave extending, the same method can be applied for the next characteristic wave extending as shown in Figure 1. The right-hand side extending method is quite similar to the left-hand side extending. In addition, we have limited the scale and amplitude of extending the nearest characteristic wave at the end of the real signal. This is especially helpful to analyze the signal with a lot noise in which case it is hard to decide the real extending characteristic wave. It is also efficient to analysis the SAR internal wave signal with strong asymmetric waveform.

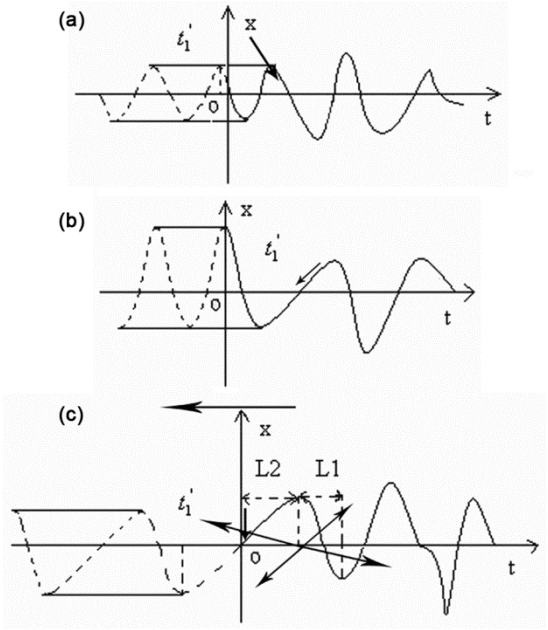

Fig. 1 — Methods for extending points

Results

Time series decomposition

The paper examined the same time series as that of Huang and Zhao[29], which were superposed to have three harmonics,

$$X(t) = \text{HF+MF+LF} = -0.5\cos(3\omega t) + 0.5\cos(\omega t) + \sin(\omega t/4) \quad \ldots (17)$$

Where $\omega = 1\,Hz$, t=0~10s. The time series decomposition results by EMD with extending method are shown in Figure 2. The dotted lines of Figures 2(a - c) stand for IMF1-IMF3, while the solid lines stand for HF, MF and LF. The three harmonics are well decomposed from original signal $X(t)$. The frequency becomes lower and lower from IMF1 to IMF3. In Figure 2(d), the reconstruction using the IMFs is shown in a dotted line, while the original data is shown in a solid line. The two lines are nearly the same with relative error of 1 %, which means the decomposition of data is perfect.

In order to compare the method with Huang and Zhao's, the results of FEM are compared with that of EEM (cf. Fig. 7)[29] at two values of t, that is t = 0, and 10. The two values of the IMF2 approach 0.5, which are the results of the MF's, while the two values in the EEM method approach 0.2. As for the results of the IMF3, the two values approach 0, which are the results of LF's, while the values in the EEM method approach 0.2. Above comparision suggest that the FEM is better than the EEM.

The paper investigates another classical nonlinear example with the Rossler equations:

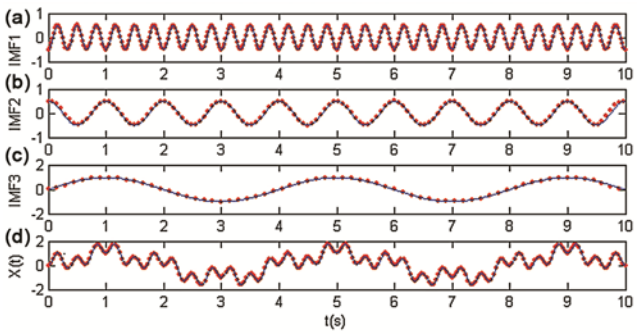

Fig. 2 — IMF1 (dotted line) and HF (solid line) (a), IMF2 (dotted line) and MF (solid line) (b), IMF3 (dotted line) and LF (solid line) (c), the reconstruction of the signal (solid line) and the data (dotted line) (d)

$$\begin{cases} \dfrac{dX}{dt} = -(Y+Z) \\ \dfrac{dY}{dt} = -(X+\alpha Y) \\ \dfrac{dZ}{dt} = \beta + Z(X-\gamma) \end{cases} \quad \ldots (18)$$

The parameters are taken as the same as those of Huang and Shen[11], *i.e.* $\alpha = 0.2, \beta = 0.2, \gamma = 3.5$, and the initial conditions $\{X(0); Y(0); Z(0)\} = \{-2; 3; 0\}$. The calculated numerical value of X is given in Figure 3(a), and the solution in three-dimensional space is shown in Figure 3(b). Figures 3(a & b) indicate that the signal needs to be rotated at twice the simple frequency to complete a full period, *i.e.* it contains two time scales. The decomposed IMFs and their residues are shown in Figure 4. We do get the expected two time scales. Compared with Huang and Shen (cf. Fig. 10)[11], Huang and Zhao (cf. Fig. 6)[29], the IMFs obtained with FEM are identical to that of Huang and Shen and EEM, and better than MPM. Because the waveform of the signal is far from symmetrical at any extrema, IMFs obtained with MPM have unavoidable end effects and have some oscillatory surges at the end points.

Finally, the method is also examined by the Lorenz equations:

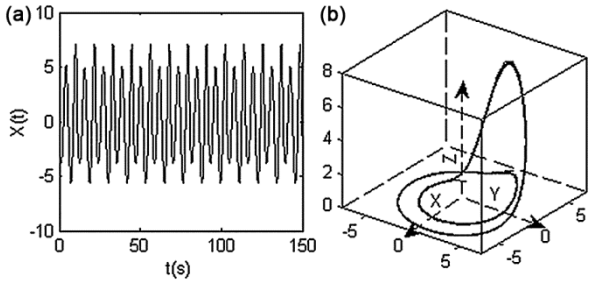

Fig. 3 — X-component (a) and phase diagram (b) for the Rossler equations

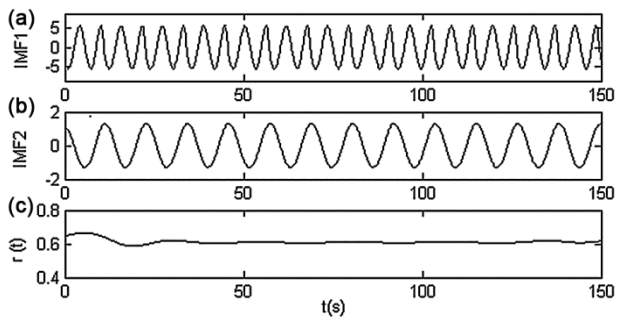

Fig. 4 — IMF1 (a), IMF2(b) and residue (c) for the Rossler equations

$$\begin{cases} \dfrac{dX}{dt} = -\sigma X + \sigma Y \\ \dfrac{dY}{dt} = rX - Y - XZ \\ \dfrac{dZ}{dt} = -bZ + XY \end{cases} \quad \ldots (19)$$

The parameters are taken the same as those of Huang and Shen[10], i.e. $\sigma = 10, b = 3, r = 20$, and the initial conditions $\{X(0); Y(0); Z(0)\} = \{10; 0; 0\}$. The numerical solution depicts a spiral motion converging to one of the point attractors at $(-\sqrt{57}, -\sqrt{57}, 19)$ as shown in Figure 5(a). The x-component is shown in Figure 5(b). Huang and Shen[10] have analyzed the x-component's Fourier spectrum which shows a sharp peak at 1.4 Hz and its harmonics at 2.8 Hz. However, the two IMF components given by them do not show this relation correctly, and IMF1's frequency is about 1.4 times IMF2's frequency. The IMFs with FEM are shown in Figure 6. In Figure 6, IMF1's frequency is twice that of IMF2 indicating a perfect result. Therefore, FEM gives a better result than that of Huang and Shen[10].

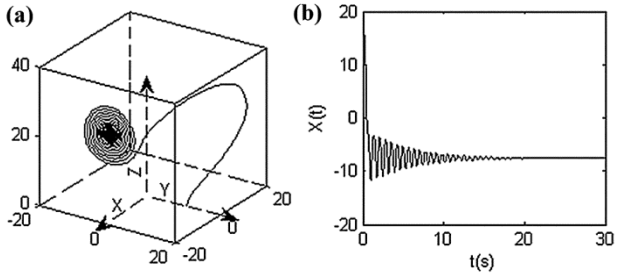

Fig. 5 — Phase diagram (a) and x-component (b) for the Lorenz equations

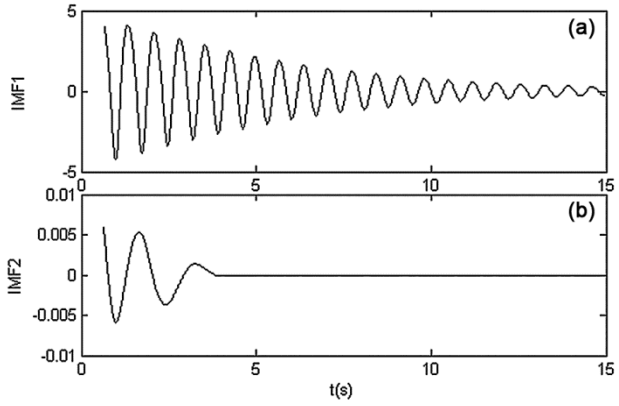

Fig. 6 — IMF1 (a) and IMF2 (b) for x-component

Internal wave temporal series decomposition

EMD is also used to study oceanic waves[20,21,30]. In this paper we use EMD with the proposed FEM method to extract nonlinear internal wave from SAR imagery. The SAR image used in this study is from ERS1 (see Fig. 7) and the studied data is the profile line AB, which the internal wave propagating from A to B. It was acquired at 10:29 on July 16, 1998. The center of the image is located at 20.01° N, 120.17° E, which covers the Luzon Strait in the southern part of the East China Sea. The size of the image is about 100 km x 100 km, and the pixel size corresponds to 12.5 m. Clearly, we can see an internal wave is propagating southwestward.

We took a data line AB from Figure 7, and decomposed the signal into 10 IMFs. We calculated the normalized deflection of each IMF based on the equation (2). The normalized deflection results from IMF1 to IMF10 are 0.0834, 0.0446, 0.0589, 0.0288, 0.0181, 0.0053, 0.0305, 0.7269, 0.0031 and 0.0004, respectively. We can see that IMF8's deflection is maximum, which means IMF8 contains the largest energy and stands for internal wave component[28].

We present IMF8 together with the original data in Figure 8. The original data contains lots of noise. However, with the FEM method proposed in this paper, the internal wave signal can be extracted and are clearly shown in Figure 8b. We also find that the wave packet consists of at least 14 solitons. The fastest soliton with largest amplitude will move in front of the wave packet when lots of solitons travel together[4], which means the amplitude of wave gets larger and larger, the speed of soliton becomes faster and faster when the internal wave propagate from A to B. Therefore, this decomposition gives us a meaningful and physical result. This result is agreement with the previous result given by wavelet method and holds the better waveform especially at the end of the signal[31]. It also proves that EMD with FEM can break down a series with a lot of noise into IMFs successfully. What we shall emphasize here is that the using of FEM for long signals with much maxima or minima decomposition can get better results.

We have also applied the EMD with FEM for other internal wave temporal series decomposition and found that this method is a power tool for internal wave signals detection. Figures 9 & 10 give us another two examples. Figure 9 contains some dark slicks and only one soliton, which looks like a white band in the left-top side of the image. The original intensity values across AB are shown in Figure 9(b) and the 4th component IMF4 with EMD is show in Figure 9(c). Figure 10 is a little different from Figure 8 and Figure 9, because Figure 10(a) is a calibrated image. We can see the normalized radar

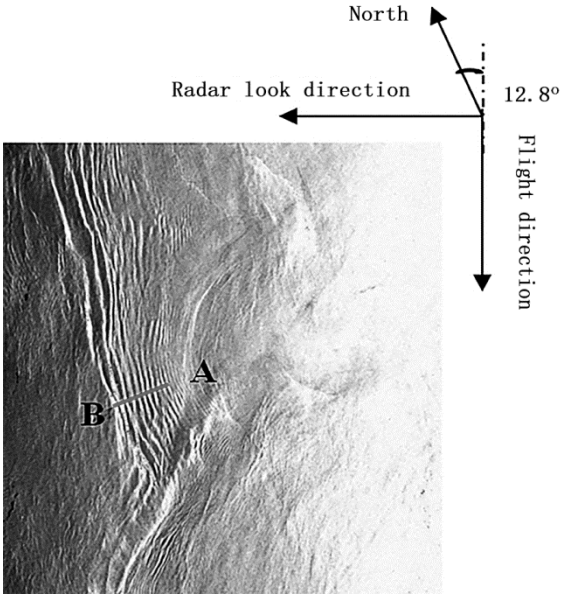

Fig. 7 — SAR imagery of Luzou Strait and the studied data line AB

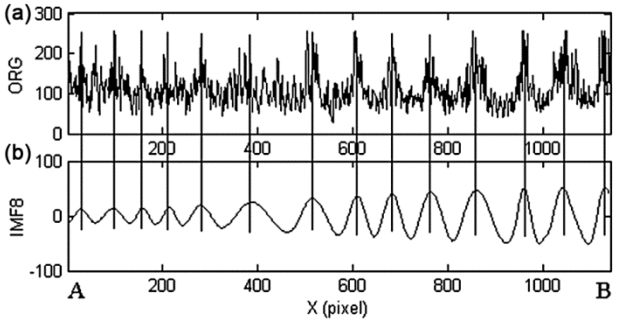

Fig. 8 — Original intensity values ORG across AB and the 8th component IMF8

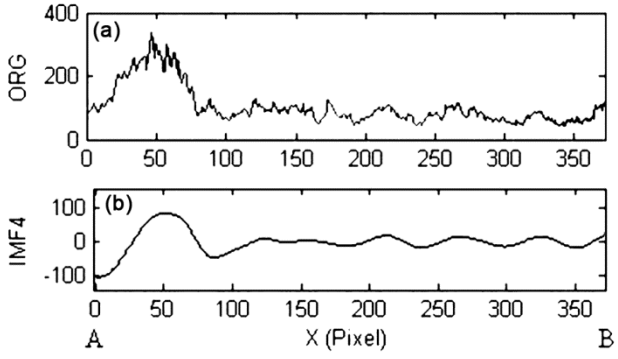

Fig. 9 — The SAR image (a), original intensity values ORG across AB (b) and the 4th component IMF4 (c)

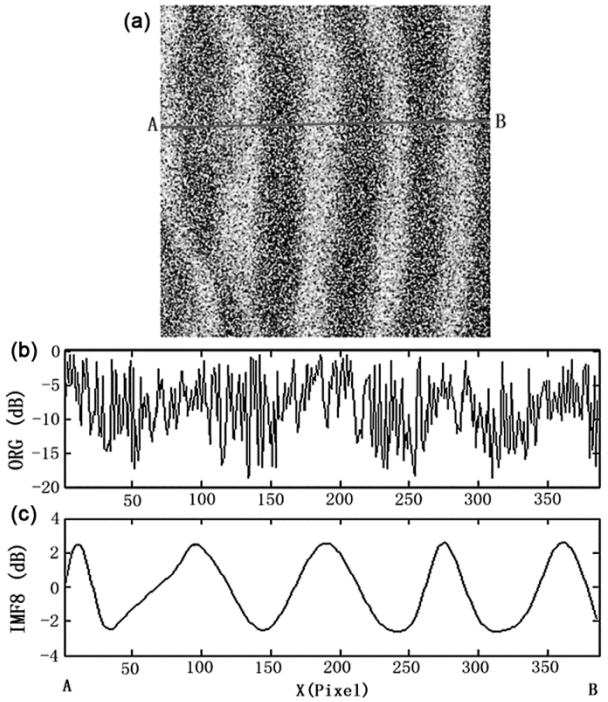

Fig. 10 — The calibrated SAR image (a), the NRCS of internal wave signal across AB (b) and its 8th component IMF8 with EMD (c)

cross section (NRCS) of internal wave signal in Figure 10(b). We applied the EMD with FEM for this internal wave signal decomposition and found that the 8th IMF8 stands for internal wave component, which is shown in Figure 10(c). Then we can see that this method can detect internal wave signal in a convenient way.

Conclusion

One improved method based on EMD with FEM and a criterion based on the theory that the max-normalized deflection stands for the largest energy is introduced for internal wave signal detection in this paper. The method could handle the end effects of EMD. The comparison shows that for symmetrical series' decomposition, the method is more feasible and more precise. This is very helpful for us to analyze the nonlinear data and detect the internal wave signals in the SAR images.

Acknowledgements

This work is supported by the Natural Science Foundation (Grant No. 41606107), We would like to thank Remote Sensing Ground Station of China, Chinese Academy of Sciences (CAS) for providing the SAR images. We also would like to thank the anonymous reviewers' comments to improve the original manuscript.

References

1 Fan Z S, Research Fundamentals of Ocean Interior Mixing, (China Ocean Press, Beijing), 2002.

2 Cai S Q, Long X M & Gan Z J, A method to estimate the forces exerted by internal solitons on cylindrical piles, *Ocean Engg*, 30 (2003) 673–689.

3 Zhao Z X, *A study of nonlinear internal wave in the northeastern South China Sea*, Ph.D. Thesis, University of Delaware, America, 2005.

4 Alpers W, Theory of radar imaging of internal waves, *Nature*, 314 (1985) 245–247.

5 Li X F, Clemente-Colon P & Friedman K S, Estimating oceanic mixed layer depth from internal wave evolution observed from Radarsat-1 SAR. *J Hopkins Apl Tech D*, 2l (1) (2000) l30–135.

6 Fan K G, Huang W G, Gan X L & Fu B, Retrieving internal wave surface currents from SAR image, *J Remote Sens*, 14 (1) (2010) 122-130.

7 Alpers W, He M X, Zeng K, Guo L F & Li X M, The distribution of internal waves in the East China Sea and the Yellow Sea studied by multi-sensor satellite images. *Proc. 2005 IEEE International Geoscience and Remote Sensing Symposium*, (Seoul), 2005, pp. 4784-4787.

8 Zheng Q A, Susanto R D, Ho C R, Song Y T & Xu Q, Statistical and dynamical analysis of generation mechanisms of solitary internal wave in the northern South China Sea. *J Geophys Res*, 112 (C3) (2007), pp. C03021, doi: 10. 1029/2006JC003551

9 Le Caillec Jean Marc, Study of the SAR signature of internal waves by nonlinear parametric autoregressive Models, *IEEE T Geosci Remote*, 44 (1) (2006) 148-158.

10 Huang N E, Zheng S, Steven R L, Manli C W, Hsing H S, *et al*., The empirical mode decomposition and the Hilbert spectrum for nonlinear and non-stationary time series analysis, *Proc R Soc Lond A*, 454 (1998) 903-995.

11 Huang N E, Zheng S & Steven R L, A new view of nonlinear water waves: the Hilbert spectrum, *Annu Rev Fluid Mech*, 31 (1999) 417-457.

12 Chen Y & Feng M Q, A technique to improve the empirical mode decomposition in the Hilbert-Huang transform, *Earthq Eng & Eng Vib*, 2 (1) (2003) 75–85.

13 Huang N E & Wu Z, A review on Hilbert-Huang transform: Method and its applications to geophysical studies. *Rev Geophys* 46 (2) (2008) 3043-3061.

14 Ditommaso R, Mucciarelli M, Parolai S & Picozzi M, Monitoring the Structural Dynamic Response of a Masonry Tower: Comparing Classical and Time-Frequency Analyses, *B Earthq Eng*, 10 (4) (2012) 1221–1235.

15 Barnhart B L & Eichinger W E, Analysis of Sunspot Variability Using the Hilbert-Huang Transform, *Sol Phys*, 269 (2) (2011) 439–449.

16 Nakariakov V M, Inglis A R, Zimovets I V, Foullon C, Verwichte E, *et al*., Oscillatory processes in solar flares. *Plasma Phys ControlFusion*, 52 (12) (2010) 124009.

17 Boudraa A O & Cexus J C, EMD-Based Signal Filtering, *IEEE T Instrum Meas*, 56 (6) (2007) 2196–2202.

18 Huang N E & Shen S S P, *Hilbert-Huang Transform and its Applications*, (World Scientific, London), 2005.

19 Flandrin P, Rilling G & Gonçalves P, Empirical Mode Decomposition as a Filterbank, *IEEE Signal Proc Let*, 11 (2) (2003) 112–114.

20 Huang N E, Long S R & Shen Z, The Mechanism for Frequency Downshift in Nonlinear Wave Evolution, *Adv Appl Mech*, 32 (1996) 59–111.

21 Huang N E, Shen Z & Long R S, A New View of Nonlinear Water Waves-The Hilbert Spectrum, *Annu Rev Fluid Mech,* 31 (1999) 417–457.

22 Wu Z & Huang N E, A Study of the Characteristics of White Noise Using the Empirical Mode Decomposition Method, *Proc Math Phys Eng Sci*, 460 (2046) (2004) 1597–1611.

23 Hariharan H, Gribok A, Abidi M A & Koschan A, Image Fusion and Enhancement via Empirical Mode Decomposition, *J Pattern Recogn Res*, 1 (1) (2006) 16–31.

24 Chang J C, Huang M Y, Lee J C, Chang C P & Tu T M, Iris Recognition with an Improved Empirical Mode Decomposition Method, *Opt Eng*, 48 (4) (2009). doi:10.1117/1.3122322.

25 Parey A & Pachori R B, Variable cosine windowing of intrinsic mode functions: Application to gear fault diagnosis, *Measurement*, 45 (3) (2012) 415–426.

26 Pigorini A, Casali A G, Casarotto S, Ferrarelli F, Baselli G, *et al*., Time-frequency spectral analysis of TMS-evoked EEG oscillations by means of Hilbert-Huang transform, *J Neurosci Methods*, 198 (2) (2011) 236–245.

27 Pachori R B, Discrimination between ictal and seizure-free EEG signals using empirical mode decomposition, *Res Lett Signal Process*, (2008) doi:10.1155/2008/293056.

28 Yang J, Zhou C & Huang W, Study on Extracting Internal Wave Parameter of SAR Images, *Remote sens techno appl*, 15 (1) (2000) 6-9.

29 Huang D, Zhao J & Su J, Practial implementation of Hilbert-Huang Transform algorithm, *Acta Oceanol Sin*, 22 (1) (2003) 1-14.

30 Remoissenet M, *Waves called sollitons: concepts and experiment*, 2nd revised and enlarged edn, (Springer-Verlag Berlin Heidelberg, New York) 1996, pp.107-116.

31 Fan K G, Zhou X Z, Xu Q, Fu B, Han L, *et al*., *Study on Synthetic Aperture Radar internal wave*, (China Ocean Press, Beijing) 2016.